Journal of Marine Science and Technology

Volume 31 | Issue 4 Article 16

# The Pre-Processing of WT Blade Images by SS and Bilateral Filter with Machine Learning Frameworks

Joy Iong-Zong Chen
*Department of Electrical Engineering, Da-Yeh University, No. 168 University Rd., Dacun, Changhua 51591, Taiwan*, jchen@mail.dyu.edu.tw

Chien-Yeh Lee
*Department of Electrical Engineering, Da-Yeh University, No. 168 University Rd., Dacun, Changhua 51591, Taiwan*

Wien-Chieh Lo
*Department of Electrical Engineering, Da-Yeh University, No. 168 University Rd., Dacun, Changhua 51591, Taiwan*



## Recommended Citation

Chen, Joy Iong-Zong; Lee, Chien-Yeh; and Lo, Wien-Chieh (2023) "The Pre-Processing of WT Blade Images by SS and Bilateral Filter with Machine Learning Frameworks," *Journal of Marine Science and Technology*: Vol. 31: Iss. 4, Article 16.
DOI: 10.51400/2709-6998.2724
Available at: https://jmstt.ntou.edu.tw/journal/vol31/iss4/16

RESEARCH ARTICLE

# The Pre-processing of WT Blade Images by SS and Bilateral Filter with Machine Learning Frameworks

Joy Iong-Zong Chen*, Chien-Yeh Lee, Wien-Chieh Lo

Department of Electrical Engineering, Da-Yeh University, No. 168 University Rd., Dacun, Changhua 51591, Taiwan

**Abstract**

**This paper discusses the motivation behind turbine migration and addresses the challenges of using NN (neural network) computing systems. Moreover, it focuses on high-dimensional data from WT (wind turbine) blades. The three key aspects addressed in this study are turbine migration, overfitting, and strict feature selection. To evaluate the performance of the machine learning system, the study considers the characteristics of WT blades, specifically the similarity in blade color and the differences in shape. The authors apply pre-processing techniques, in particular a bilateral filter, in conjunction with the SS (selective synthesizer) of blade fouling patterns. The SS method adopts the framework of ResNet50 to evaluate the computational efficiency. The experimental results show that the introduction of the SS method for feature selection improves the accuracy rate of the NN model to over 92 %. For data validation, the study employs the YOLO (You Only Look Once) deep learning framework. Specifically, YOLOv4-Tiny is used due to its trade-off between recognition speed and accuracy. In addition, YOLOv4-Tiny was integrated with the Nvidia Jetson Nano edge computing hardware. Overall, the article focuses on the use of machine learning techniques, such as preprocessing and feature selection, to improve the performance of NN computing systems in analyzing high-dimensional data from WT blades. The authors validate their approach using the YOLO framework, specifically YOLOv4-Tiny, and highlight the integration with Nvidia Jetson Nano for edge computing.**

*Keywords:* Bilateral filter, Selective synthesizer, WT (wind turbine) blades, YOLOv4-Tiny model

## 1. Introduction

To maintain power generation efficiency and safe operation of WT (wind turbine), regular inspection of WT blades is necessary. According to recent market research, the revenue generated by the widespread use of UAVs (Unmanned Aerial Vehicles) is expected to exceed $8.5 billion by 2027. In addition, the UAV-based architectures are explored for the development and implementation of next-generation technologies such as 5G, V2X (vehicle-to-everything) communications, etc. [1]. The current status of wind power development in Taiwan, at present an important indicator of the country's energy policy is that the government hopes to achieve the goal of a non-nuclear homeland by 2025. In 2025, the proportion of renewable energy power generation can account for more than 20 % of the country's total power generation. The benefits of installations are more economical in scale, and solar power generation faces problems such as power generation efficiency land acquisition difficulties, and the reduction of wholesale electricity prices. Currently, the demand for construction is gradually slowing down, and wind power generation is gradually becoming a development due to issues such as offshore wind turbines. Renewable energy is an important option. With international wind turbine manufacturers, Taiwan has become the focus of offshore wind power development in the Asia region, which was discussed in the literature [2].

The blade is one of the most important components embedded into the WT skeleton. Compared

Received 15 April 2023; revised 12 November 2023; accepted 13 November 2023.
Available online 15 December 2023

* Corresponding author.
E-mail addresses: jchen@mail.dyu.edu.tw (J.I.-Z. Chen), D1003004@cloud.dyu.edu.tw (C.-Y. Lee), lowctwan@gmail.com (W.-C. Lo).

https://doi.org/10.51400/2709-6998.2724

with other wind turbine components, the test or certification requirements for wind turbine blades are the most stringent. Different wind farm environments present different challenges. In European wind farms, when it is extremely cold in winter, the blades can freeze and not rotate. At the wind farm located in Taiwan, the blades may rotate too fast and cause thermal damage when a typhoon is raging in summer. It is known that the risk could happen surrounding the WT, thus, addressing the event of exactly inspecting the safety of WT blades is a critical issue. Recently, machine learning techniques have been applied to the inspection of WT blades that followed. The paper by [3] empirically investigates the performance of state-of-the-art deep learning algorithms, namely, YOLOv3, YOLOv4, and Mask R−CNN for defect detection and classification by type. The paper proposes new performance evaluation measures suitable for defect detection tasks, and these include Prediction Box Accuracy, Recognition Rate, and False Label Rate. Experiments were carried out using a dataset, provided by the industrial partner, that contains images from WTB inspections. A YOLOv4-based wind turbine blade crack detection method is proposed in [4] which firstly establishes the WT blade crack image dataset, then the anchor box parameters in YOLOv4 are optimized by $K$-means$^{++}$ algorithm to make the anchor box parameters match the crack defect size. Besides, a novel SHM (structural health monitoring) methodology that takes advantage of the fact that the WT blades are nominally identical in structural properties is proposed in [5]. The methodology is used to predict the edge frequencies of one blade given that of another after these relationships between the pairs of blades have been learned when the blades are in a healthy state. Recently, a fast WT defect detection model has been proposed with a Cascade Mask R−CNN (Region Convolutional Neural network) [6]. Instead of the standard convolution in the backbone network of Cascade Mask R−CNN, a depth separable convolution is used to minimize the computational cost. The experimental results announced that the proposed WT blade defect detection and classification model shows better performance with 82.42 % MAP, and 97.8 % classifier accuracy.

To capture wind energy and to propose an automated visual inspection system for WTB are completed in [7,8], respectively. In the former, the human mind must rely on both hands to perform actions or designations, and an improved YOLO (You Only Look Once) model is developed with a deep learning framework in the latter. To achieve practically acceptable detection accuracy for small-sized defects on WTB, they utilized a database of 23,807 images annotated with three types of defects: cracks, oil, and sand inclusions. The comprehensive review in [9] provides the state-of-the-art embedded sensors, communication technologies, computing platforms, and machine learning techniques used in autonomous UAVs. The key performance metrics along with operating principles and a detailed comparative study of the various technologies are also studied and presented. Besides, to test the applicability of acquiring accuracy, in [10] the random forest machine learning algorithm for classification processing is presented. It is applied with radiometric features and geometric characteristics derived from covariance features (curvature, omnivariance, flatness, linearity, surface variance, anisotropy, and normalized terrain surface) of points. There a DL-based method for UAV detection in pulse-Doppler radar is proposed in [11]. It considers the position offset of the target to the center of the local window which method designs a CNN with not only a classification head but also a regression head to achieve the precise location of the target for UAV detection. Moreover, based on background removal a preprocessing method is proposed in [12] to overcome the drawbacks of image blurring occurring at WT blades. The idea of the method is to carry out image segmentation to get the background part, and then the intensities of pixels in the background part are replaced by the same value. The robustness of the parameters and the capability of image stitching of the proposed method is well verified. For solving the existing problems of stability, sensor installation, and data storage and processing. A novel blade inspection method based on deep learning and unmanned aerial vehicles is proposed in [13]. Onsite visual surface inspection is still the most common inspection method since most studies of WT blade inspection focus attention on acquired sensor signal processing. It is inefficient and requires a long downtime. The contents of [14] put forward a set WT blade detection method based on an artificial intelligence image recognition system. A lot of image acquisition processing is carried out for WT blades in service with the help of high-definition camera array and image recognition software. Eventually, the automatic detection of blade surface defects is realized.

Based on the vibration signal of the shaft bearings during multi-SVM (support vector machine) process, a multi-class SVM and a CNN were employed for fault diagnosis and the RUL (remaining useful life) prediction of the shaft bearings used in WT [15]. In addition, the authors in [16,17] also applied a similar algorithm framework to detect WT blade defects and obtained similar and excellent research results. The effectiveness of the YOLO algorithm in the detection

of WT blades has never been found in the aforementioned studies. Based on the self-assessment of the risk analysis score sheet and the re-assessment by the director of the fire department in the onshore wind power area and the business unit, the experts assessed the higher hazard risks including blade structure breakage (risk level>3) and falling (risk level>3), unit structure Collapses (risk level>3) and adjacent site fires cause structural damage to wind power. Due to structural damage or deterioration, the blades are prone to breakage, cracking, falling, and other risk factors. After falling, it is easy to cause damage to power facilities and cause electrical fires. Therefore, it is recommended to implement regular inspections of WT blades [18,19].

Specifically, in this study, an algorithm is proposed not only to overcome the problems with high-dimensional data and data overfitting but also the SS (selective synthesizer) scheme is used to find solutions and address the limitation of NN (neural network) computation for recognition the WT blades possible damage. On the other hand, the motivation of this study is to propose a novel method by using of Bilateral filter [24] for image pre-processing to improve the effectiveness and efficiency of TW blade detection and identification. The provided research data is screened for data elements. That is, this investigation is mainly based on the image data of WT blade contamination identification and the detection of WT blades. The classification of hazards such as "blade structure" and "unit structure" in "*Hazard Identification and Risk of Personnel in Adjacent Areas*" by structure and a high-correlation pre-processing study is proposed. Executed by a host computer with image processing unit GPU (graphical processing unit) computing speed, and a large number of original data rooms come from commercial wind farms [21,22], and through the website [9] which provides images of WT blade. Thus, the WT blade identification practice can enter the mold Group establishment and verification phase. The WT blade image pre-processing detection algorithm and development results proposed in this article, it is enough to help the wind farm blade mutation identification accuracy successfully reach more than 90 %. Traditional image preprocessing systems, whose requirements for preprocessing deep learning models, are RGB images belonging to databases of any size. Since the leaf map to be used in this investigation is not the expected data in the investigation, it is the original map provided by the external undetermined form, and it is believed that the content of the map contains various leaf forms, not the only one.

Therefore, to improve the accuracy of the final WT blade defect identification and reduce the loss rate of data training, it is necessary to significantly improve image uniformity and obtain the benefits of peer-to-peer training. The captured images usually have different image features. If the training process produces gradient dissipation or gradient divergence, the identification number may not be converted correctly [22]. This image pre-processing platform is established to solve this problem.

The rest of the paper is divided into four sections described as follows, after the introduction section, the problems and requirements of land WT blades are discussed in section II. In section III the pre-processing of the WT blades with normal (A) and damaged (B) WT is investigated. Apart from this, the discussion of the Bilateral filter and the SVD techniques for the proposed DNN-LSTM framework is presented in section IV. Eventually, the experiments plus results and a brief conclusion are presented in section VI.

## 2. Description of problems and requirements

In this section, the critical issues of the possible fact caused by the WT blade will be explained in detail. Hazard identification and risk assessment of land-based WT blades will also be discussed. Many useful theoretical techniques are also included, such as the SS scheme.

### *2.1. Discussion of possible problems happen in damage of WT blades*

Through the risk analysis method, the damage of WT blades in the land area is used to determine the risk factors of damage to the adjacent areas. Through the disaster risk analysis, the disaster risk factors with high destructive force are locked, and then the high risk factors are analysed for the application of disaster prevention and early warning in the wind power system with benefits. Therefore, the prerequisite of this study is first to understand the results of the hazard from the craft of WT blade, which includes,

(1). *The Identification of the factors*,

Investigate all possibilities of blade fall, compile and list all conditions for risk assessment, then discuss with experts and scientists, eliminate, confirm and integrate all equipment and processes that need to be assessed.

(2). *The Identification of possible hazards and consequences*

Define the classification or type of potential hazards according to the characteristics of each type of hazard, and identify all potential hazards, their

causes and the reasonable and most serious consequences according to the accident (risk) classification as hazard identification.

(3). *The assessment of the risk of all hazards,*

The following factors must be taken into account when assessing the possibility of establishing a reference example for the possibility classification benchmark, such as the level of hazard, the frequency, and duration of exposure to the hazard, etc. For example, if the frequency of exposure or duration of exposure is higher, the likelihood of a hazardous event will be higher. For example, if the frequency of exposure is higher or the duration of exposure is longer, the likelihood of a hazard event will be higher.

(4). *The assessment of the hazard risk severity,*

The following factors must be considered in evaluating the severity to establish a reference example of the severity grading benchmark.

(a) The parts of nearby people who may be injured or affected, the number of people injured, etc.
(b) The degree of injury, such as death, permanent disability, temporary disability, first aid treatment, etc.

Finally, the various hazard factors that can cause WT blades to fall are listed separately for each possible hazard type, and the situation or process in which the consequences can occur is also described in detail. The severity and risk levels are evaluated, and a risk assessment table is produced in Table I.

Generally speaking, in the technical application framework of machine learning, if it needs to be applied to dynamic image recognition, YOLO neural modules are the best choice. In addition, to reduce the dynamic error caused by dynamic orientation, the YOLO module can avoid the problem of excessive loss of image data caused by the above-mentioned error. Based on the above discussion, some measures have been taken for this research, because the goal to be achieved according to this research is to identify the fouling of WT blades in an instantaneous and dynamic environment. Therefore, this research uses the YOLO module in the training process of the actual verification image data, on the one hand, it can reduce the signal training loss of the dynamic error. On the other hand, it is also expected that in the real-time and dynamic condition environment, more accurate training modules can be obtained and the accuracy can be improved, which is helpful to the research object. On the other hand, 3 points can be made about the advantages of YOLO. The first point is that YOLO has a strong spatial constraint on the bounding box. If there are more than two objects that are very close in space, the model cannot be effectively trained. Secondly, when the trained model is asked to predict other new objects or objects with odd proportions, it may not be able to frame them well. Part of the reason for this is that YOLO itself has many layers of pooling (downsampling). The last feature is used to predict the bounding box, which is relatively coarse in space compared to the original image. Finally [26], points out that when calculating the RoI (Region of Interest), if a small object is just a little bit off, the localization error will have a large impact, but there is not much difference for a large object.

ResNet stands for Residual Network. Resnet-50 is used to describe the variant that can work with 50 neural network layers [27,28]. When working with deep convolutional neural networks to solve a problem related to a computer vision problem, machine learning experts are concerned with stacking more layers. These additional layers help to solve complex problems more efficiently, as the different layers can be trained for different tasks to achieve highly accurate results. While the number of stacked layers can enrich the features of the model, a deeper network can reveal the problem of degradation. In other words, as the number of layers in the neural network increases, the accuracy levels may become saturated and slowly degrade after a certain point. As a result, the performance of the model deteriorates in both training and test data.

*Table 1. Hazard identification and risk assessment.*

| Items | Hazard classification | |
|---|---|---|
| **A** | WT Unit structure | Falling、Broken、Crack、Collapse、Mechanical failure、The hazards are divided into natural disasters (typhoons, storms, strong winds, earthquakes, lightning strikes …), and so on. |
| **B** | Wind power fire | Mechanical failure、Debris falls、Falling、Ignite the field、Building disaster、Natural disasters (typhoons, storms, strong winds, earthquakes, lightning strikes, etc.) |
| **C** | WT blade structure | Component falling、Wind blade broken、Wind blade crack、Collapse、Debris falls、Mechanical failure、Natural disasters (typhoons, storms, strong winds, earthquakes, lightning strikes …) |

The application of both YOLO and Resnet-50 to the experimental process is discussed in section IV.

### 2.2. Description of the SS techniques

The best damage pattern is selected from the output end of the synthesizer as the final output of the WT blade that can cause damage, which is called SS. It can be divided into pure SS and threshold SS. The SS does not necessarily select only one optimal output destruction pattern of the WT blade but can select two or three, or even more optimal destruction patterns as output after synthesis. The selection of two (or three) a synthesizer with the best signal is called a second-order (or third-order) SS.

#### 2.2.1. Pure SS

Pure SS is to continuously monitor the received signal to select the best optimal damage pattern. In theory, it must select the possible jamming pattern with the best probability value, but in practice this is difficult to do. It can only select the jamming pattern with the highest output probability. Each branch of the SS must have its own decision algorithm, which increases the cost and complexity of the equipment.

#### 2.2.2. Threshold SS

The basic principle of the Critical Value SS is that each received damage pattern is scanned sequentially and the first scanned damage pattern greater than the Critical Value is selected as the output. As long as the damage pattern of this damage pattern probability value is still greater than the critical value, this damage type will be used as the output damage type. Otherwise the synthesizer will repeat the scan. The critical value setting can be fixed or variable. Before setting the critical value, the probability value generated by the average damage pattern of the geographical area must be fully captured. If the damage pattern is assessed in a fixed area, the fixed critical value method can be used. However, as for the non-fixed blade operation area, since the non-fixed blade operation area often moves in different regions, the average probability judgment strength of each region may not be the same. If the fixed critical value method is used, the system judgment result will be unstable and unnecessary. The switching action occurs, so the method of changing the threshold value is more suitable.

### 2.3. Ordered statistics

If there are independent random variables and a random variable whose size ranks *k-th* is selected from them, then the statistical characteristics of this random variable are what order statistics will discuss. Since the second-order (third-order) SS selects two (three) types with the strongest strength from among these items after receiving the items, and then adds the probability value of the two (three) items and outputs them with the appropriate results. Thus, the concept of ordered statistics must be used. This subsection gives a brief discussion of the distribution of single, two, and more than two-ordered statistics [23].

#### 2.3.1. Single-ordered statistic distribution

Assume that there have $n$ independent random variables, $X_1, X_2, \ldots, X_n$, which all have the same CDF (cumulate distribution function), $F(x)$, and pdf (probability density function), $f(x)$. Now arranging the $n$ random variables in the order from large to small $X_{(1)} \le X_{(2)} \le \cdots \le X_{(n)}$ where $X_{(r)}$ is the $r$-th ordered variate. Thus, the event is given as the expression [18],

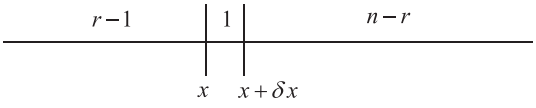


It is known that in the range of $X_i \le x$ where has $r-1$, and just one and $n-r$ located during the duration of $x < X_i \le x+\delta x$ and $X_i > x+\delta x$, respectively. Consider that $\delta x$ is a very small value, hence the probability for the event of $x < X_{(r)} \le x+\delta x$ can be determined as

$$P(x < X_{(r)} \le x+\delta x) = \frac{n!}{(r-1)!(n-r)!}[F(x)]^{r-1} [1-F(x+\delta x)]^{n-r} \times [F(x+\delta x)-F(x)] + O\left((\delta x)^2\right) \quad (1)$$

where $O((\delta x)^2)$ represents the probability value for two or larger than two $X_i$ which fall during the interval of $(x, x+\delta x]$, dividing both of the two sides of Eq. (1) with $\delta x$,and the probability value of $X_{(r)}$ over $(1 \le r \le n)$ can get as

$$f_r(x) = \lim_{\delta x \to 0}\left\{\frac{P(x < X_{(r)} \le x+\delta x)}{\delta x}\right\} = \frac{n!}{(r-1)!(n-r)!}[F(x)]^{r-1}[1-F(x)]^{n-r} f(x) \quad (2)$$

where the variable $\delta x$ is considered as approaching zero. Therefore, by substituting $r = n$ into Eq. (2) the pdf for the maximum variable of $X_{(n)}$ can be determined as

$$f_n(x) = \frac{n!}{(n-1)!(n-n)!}[F(x)]^{n-1}[1-F(x)]^{n-n} f(x) = n[F(x)]^{n-1} f(x) \quad (3)$$

*2.3.2. Joint distribution of multiple-ordered statistics*

In this subsection the derivation of jpdf (joint pdf) for two ordered variables, $X_{(r)}$ and $X_{(s)}$ $(1 \le r < s \le n)$, is provided. The event of $\{x_r < X_{(r)} \le x_r + \delta x_r, x_s < X_{(s)} \le x_s + \delta x_s\}$ is analyzed as the following expression,

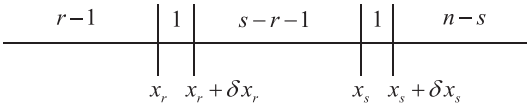


where has the number of $r-1$ for variable $X_i$ occupies the range of $X_i \le x_r$. One of $X_i$ is just located in the duration of $x_r < X_i \le x_r + \delta x_r$, and there $s-r-1$ of $X_i$ are dwelling on the interval of $x_r + \delta x_r < X_i \le x_s$. Besides, one of $X_i$ is just located at the interval of $x_s < X_i \le x_s + \delta x_s$, and there have $n-s$ of $X_i$ limited in $X_i > x_s + \delta x_s$. Onward, after the variables of $\delta x_r$ and $\delta x_s$ are assumed as approaching to zero, the probability of outcome for the event of can be calculated as

$$\begin{aligned} &P\{x_r < X_{(r)} \le x_r + \delta x_r, x_s < X_{(s)} \le x_s + \delta x_s\} \\ &= \frac{n!}{(r-1)!(s-r-1)!(n-s)!}[F(x_r)]^{r-1} \\ &[F(x_s) - F(x_r + \delta x_r)]^{s-r-1} \times [1 - F(x_s + \delta x_s)]^{n-s} \\ &[F(x_r + \delta x_r) - F(x_r)][F(x_s + \delta x_s) - F(x_s)] \\ &+ O\left((\delta x_r)^2 \delta x_s\right) + O\left(\delta x_r (\delta x_s)^2\right) \end{aligned} \tag{4}$$

where both of $O((\delta x_r)^2 \delta x_s)$ and $O(\delta x_r (\delta x_s)^2)$ are polynomial with higher order. On the other hand, the previous probability is conditioned on the following constrains, (A) there has two or greater than two variables $X_i$ falls into the interval of $(x_r, x_r + \delta x_r]$, (B) there is at least one variable located at the duration of $(x_s, x_s + \delta x_s]$, (C) there is at least one variable of $X_i$ located at the duration of $(x_r, x_r + \delta x_r]$ and two or more than two variables of $X_i$ dwells on $(x_s, x_s + \delta x_s]$. Next, let $\delta x_r \to 0$ and $\delta x_s \to 0$ then divides $\delta x_r \delta x_s$ for both side of equivalent in Eq. (4). The jpdf of $X_{(r)}$ and $X_{(s)}$ with the condition of $(1 \le r < s \le n)$ can be obtained as

$$\begin{aligned} f_{rs}(x_r, x_s) &= \lim_{\substack{\delta x_r \to 0 \\ \delta x_s \to 0}} \left\{ \frac{P\{x_r < X_{(r)} \le x_r + \delta x_r, x_s < X_{(s)} \le x_s + \delta x_s\}}{\delta x_r \delta x_s} \right\} \\ &= \frac{n!}{(r-1)!(s-r-1)!(n-s)!}[F(x_r)]^{r-1}[F(x_s) - F(x_r)]^{s-r-1} \\ &\quad \times [1 - F(x_s)]^{n-s} f(x_r) f(x_s) \end{aligned} \tag{5}$$

The jpdf under the condition of obtaining the largest one and the second largest one can be obtained by substituting $r = n-1$ and $s = n$ into Eq. (5). Thus, it can be expressed as

$$\begin{aligned} f_{n,n-1}(x_n, x_{n-1}) = &\frac{n!}{(n-1-1)!(n-n+1-1)!(n-n)!} \\ &[F(x_{n-1})]^{n-1-1} \times [F(x_n) - F(x_{n-1})]^{n-n+1-1} \\ &[1 - F(x_n)]^{n-n} f(x_{n-1}) f(x_n) = n(n-1) \\ &[F(x_{n-1})]^{n-2} f(x_{n-1}) f(x_n) \end{aligned} \tag{6}$$

Similarity, the derivative process can be extended to determine the jpdf for $k$ ordered variables. That is, the jpdf of ordered variables $X_{(n_1)}, X_{(n_2)}, \ldots, X_{(n_k)}$, $x_1 \le x_2 \le \cdots \le x_k$, corresponding to the ordered variables of $(1 \le n_1 < n_2 < \cdots < n_k \le n; 1 \le k \le n)$ with $k$ ordered observations can be evaluated as

$$\begin{aligned} &f_{n_1,n_2,\ldots,n_k}(x_1, x_2, \ldots, x_k) \\ &= \frac{n!}{(n_1-1)!(n_2-n_1-1)!\cdots(n-n_k)!}[F(x_1)]^{n_1-1} f(x_1) \\ &\times [F(x_2) - F(x_1)]^{n_2-n_1-1} f(x_2) \cdots [1 - F(x_k)]^{n-n_k} f(x_k) \\ &= n! \left[\prod_{j=1}^{k} f(x_j)\right] \prod_{j=0}^{k} \left\{ \frac{[F(x_{j+1}) - F(x_j)]^{n_{j+1}-n_j-1}}{(n_{j+1} - n_j - 1)!} \right\} \end{aligned} \tag{7}$$

As the previous discussion to the ordered statistic in which the WT blade damage type can be assigned as the ordered variables, for example, $X_1, X_2, \ldots, X_n$ corresponding to the blade damage type. On the other hand, the $r$-th ordered variate could be assigned as "*damaged type A*", "*damaged type B*", "*non-damaged type (c)*", and (or) "*unknown damaged type (D)*", and so on. The discussion to the classification of damaged types for WT blades is going to be presented in the later section.

*2.4. The major constrains and necessity*

In fact, there are many critical limitations of the proposed methodologies that will be discussed in this subsection.

Overall, it is known that the limitations of current knowledge in this field would include 3 critical points,

1. The acquisition of images for WT blades in real time status.
2. The limitation of the transmission bandwidth provided to the transceiver between the edge device embedded in the NVIDIA Jetson Nano Xavier and the monitoring instruments.
3. Since the environment is assumed to be too clean (without noise) in this article, the validation and prediction phases become major

obstacles in the investigation. In order to prove the results can be used as a practical method for valuable reference, certainly adds a lot of noise to simulate the situation in the factory is necessary. That is, when the environment is required for training or in the test stage, the requirement of setting up a practical environment should be considered first.

However, even there, the aforementioned constraints and concerns remain. The possible safety and emergency hazards caused by WT blades are indeed the key points when considering the operation of wind turbines. Therefore, how to really use machine learning technology and apply it deeply to the detection and maintenance of WT blades is indeed a very important public safety issue. Therefore, the research topic proposed in this article has been verified by actual experiments and found to be a feasible solution.

## 3. Pre-processing of the WT blades

The research will use the block diagram shown in Fig. 1 to complete the blade damage detection in three steps. In the first step, the acquisition of WT blades and the pre-processing after the acquisition are carried out. This includes edge detection of the blades and noise removal, then by performing normalisation with normal distribution. The more important blade characteristics are retained in the extracted blades, such as colour change, staining and/or deformation cracks. After training, the blade features are sent to the framework for confirmation. The training mode of the diagnosis and prediction framework must be set before confirmation. Of course, the parameters of the main framework and then the building of the prediction model must be determined first. In addition, it will go through the blade training and testing after the completion of the blade identification figures out in the first stage. In the final stage of this project, the evaluation of the blade identification results will be carried out. This work will use the YOLOv4 model in the confirmation process. It is expected to adopt four types of identification, from Type A to Type D damage classification. Finally, the performance evaluation of the final identification results will be determined by the schemes of R2, MSE and MA-1.

Accordingly, the pre-processing of the WT blade images is shown in Fig. 2. The original WT blade image is first sliced and the number of slices depends on the resolution degree of the edge and segments of the results. The judgement of whether it is suitable for fouling and worn blades or not is

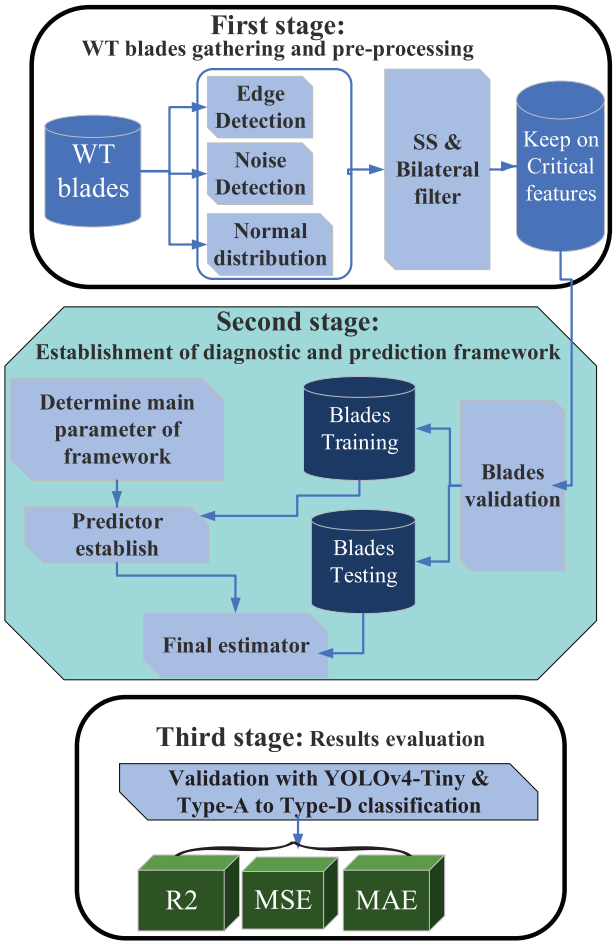


*Fig. 1. The block diagram includes three stages for the proposed project.*

made according to the results of the classification. At this moment, the different types for the classification of the damaged WT blade have been assigned 4 types as follows, "Damaged Type A", "Damaged Type B", "Non-Damaged Type (c)", and (or) "Unknown Damaged Type (D)".

Of course, the confirmation of the type of damage and (or) other items on the edge is made by calculating the probability through the SS scheme. That is, the activity selection at this time has the damage types including shape, size and type of blade crack then the obtained probability is synthesized. In addition, the normal and damaged WT blades are shown in Fig. 3, where the size of the resolution is also shown. There are many section images shown in Fig. 4 corresponding to the case of normal and damaged type of WT blades.

The determined likelihood is then given to determine if the given likelihood is appropriate. If the confirmed probability is suitable, it means that the image is worth keeping and can be used as an image for identification. Conversely, a new capture

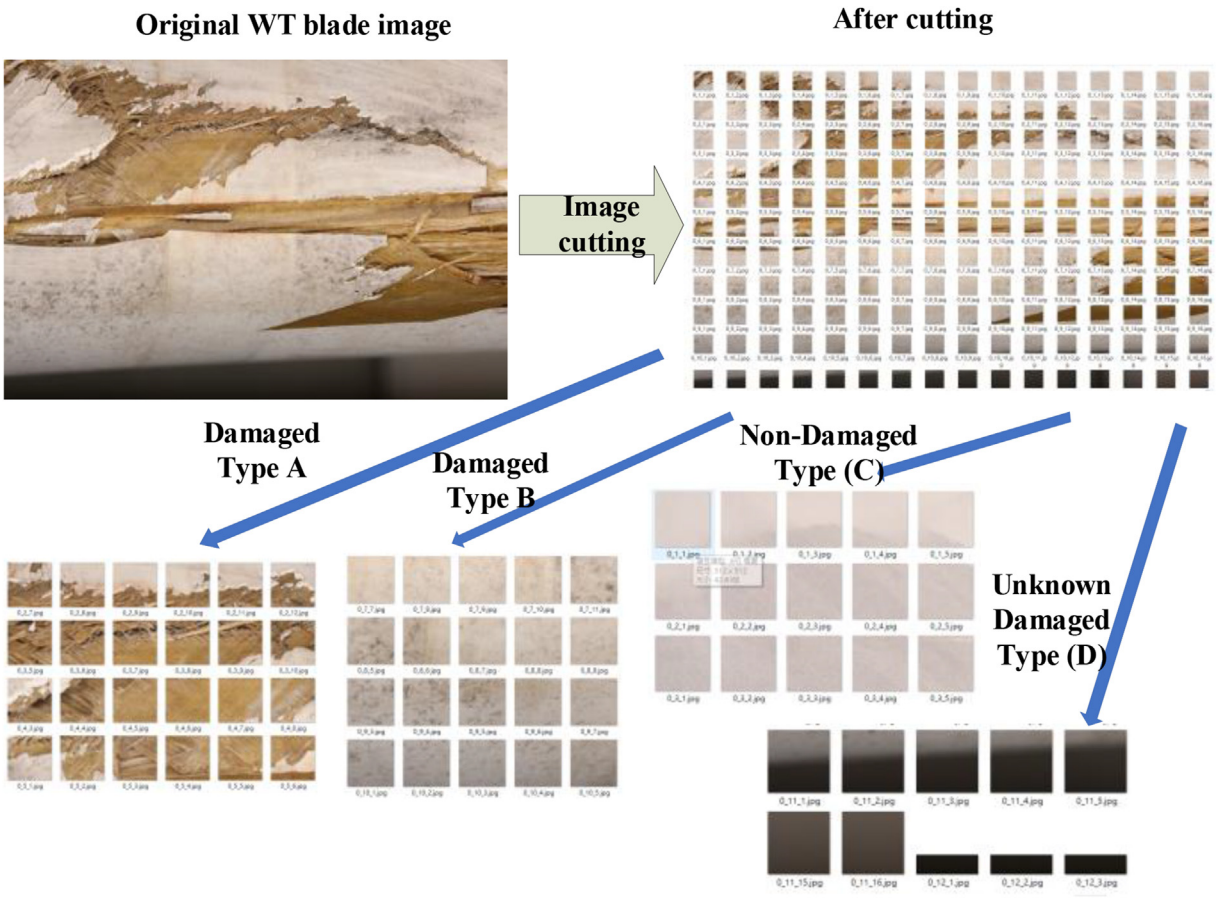


*Fig. 2. The pre-processing process of the WT blade images.*

action is performed on the WT blade image, and then the next judgement is made with a new iteration. On the other hand, the capture iteratively of performing edge and segment actions on the captured WT blade, and this previously described action has been done repeatedly until the 5 execution times are arrival. If the given blade is selectively synthesized, the identification of the WT and the

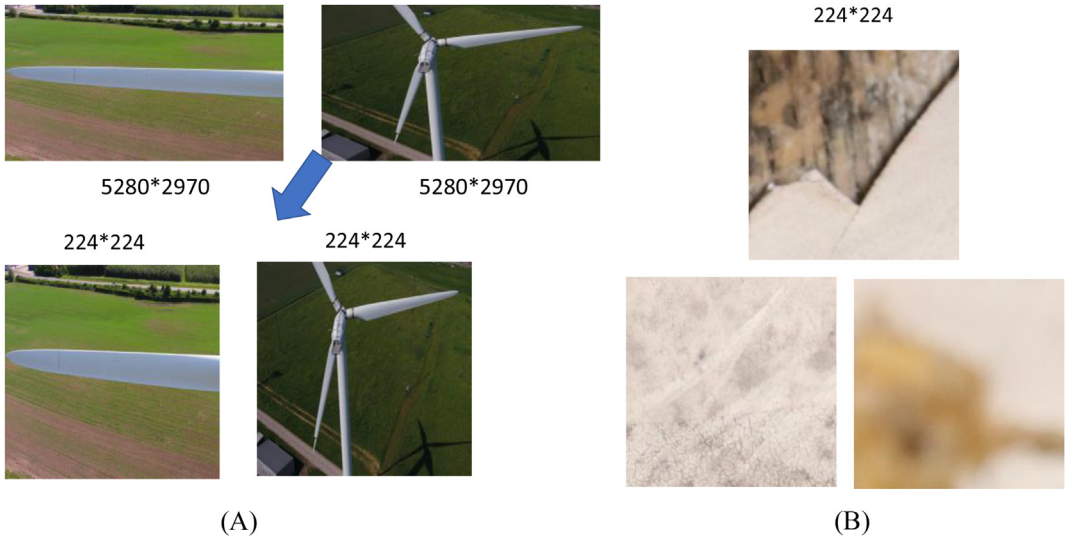


*Fig. 3. The normal (A) and damaged (B) WT blades.*

*Fig. 4. Corresponding to the case of normal and damaged type.*

blade is carried out after an appropriate probability has been given. If the given extraction edge is not suitable, bilateral filtering, edge correction and segmentation modification are performed, and then it is judged whether the corrected result of this edge is correct. This cycling process is the pre-processing process of WT blade images proposed in this study.

## 4. SS and bilateral filter

Feature selection refers to the process of reducing the number of unnecessary features before feeding them into a classifier. The feature extraction algorithm proposed in this paper relies mainly on the features of SVD. The main purpose of this technique is to achieve reliable usability for color images. Therefore, SVD is a numerical technique for decomposing input data into expected submatrices [15]. In addition, this subsection introduces the bilateral filter, which is a filter that can be used to preserve the edge and denoise an original image.

### *4.1. Description of the SVD techniques*

The feature extraction algorithm proposed in the current article, where the technique depends mainly on the features of SVD. Several feature selection techniques have been discussed and implemented so far. A perfect classifier does not need feature selection because it can ignore irrelevant features. In real time, no classifier is perfect and there is no guarantee that feature selection will improve its accuracy. The main goal of the proposed technique is to achieve reliable robustness for color images. Accordingly, SVD is a numerical technique that decomposes the input data into expected submatrices [21]. Basically, after decomposing the input image, one obtains a graph matrix with singular values for the diagonal elements. Assuming this is the input signal, it represents the left and right singular vector matrices respectively, and these singular values correspond to the energy of the signal. Rendered as a graph matrix, given as

$$\mathbf{A} = \mathbf{USV}^T \tag{8}$$

where $T$ is the transpose. Based on the SVD technique and steps described in Fig. 5.

Normally, feature extraction is the most important stage before the above-mentioned activity of image cutting, which is discussed in section III. To the best of the authors' knowledge, the proposed scheme of image clipping is a completely new method. Certainly, it must follow the steps shown in Fig. 5. Dimensionality reduction is a key technique for extracting the most important features and at the same time reducing the complexity of the processing.

### *4.2. Describe the techniques for preserve edge and denoise techniques*

A traditional filter that can preserve the edge and denoise is usually the bilateral filter. It can filter out the noise in the image data and even preserve the edge, texture, etc. of the image. This is because the noise is a high frequency signal. Therefore, the Gaussian filter will blur the edge while filtering the noise because the edge and texture are also high frequency information. So the question is, what kind of event exactly is such an excellent filter? In fact, it uses a convolution kernel (template matrix), just like

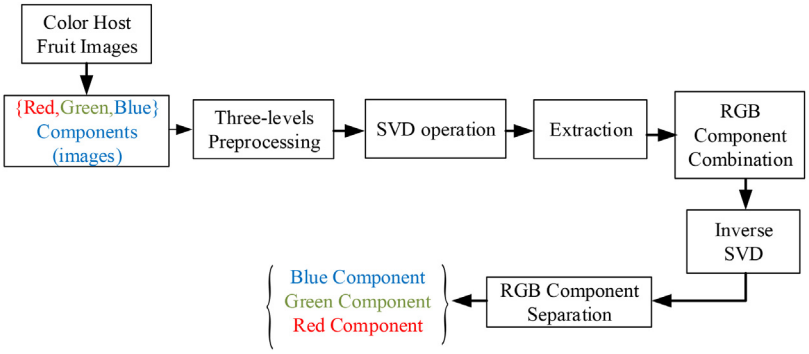


*Fig. 5. Flowchart of the extraction process of the SVD algorithm.*

the ordinary Gaussian filter. This filter is also superimposed on the pixels to be processed and the corresponding neighbouring pixels are provided. The weighted sum of the points is used as the method for the value of the new output pixel point. In simple terms, bilateral filtering is the same as Gaussian filtering, the only difference being the template matrix. Normally, the template coefficient matrix of the Bilaterial filter is obtained by dot-multiplying (element-level multiplication) the range coefficients of the Gaussian template matrix. Two filters that can be compared with each other are the Gaussian low-pass filter and the $\alpha$-truncated mean filter (the mean of the remaining pixels after removing the minimum and maximum percentages of $\alpha$ is used as the filter) [17]. The reason for this is similar to the previous description. Accordingly, in a flat area, the pixel difference is small and the corresponding value domain weight is close to 1. At this point, the spatial domain weight plays an important role, which is equivalent to directly applying Gaussian blur to this area. In the edge area the pixel difference value is large. The coefficient of the range decreases that is resulting in the decrease of the kernel function here (due to $w = r \times d$), and the less the current pixel is affected. Thus, it is able to maintain the detail information of the edge pixel. Suppress pixels with a large difference in value from the center pixel (even if you are close in space).

Onwards, the calculation method is briefly descripted following up. For each neighborhood pixel calculate its corresponding spatial coefficient and value domain coefficient first. With the multiply to obtain the total coefficient is the next step then perform weighted summation and

$$PV(i,j) = \sum_{k,l} f(k,l) w_g(i,j,k,l) \Big/ \sum_{k,l} w_g(i,j,k,l) \quad (9)$$

where the weighting factor $w_g(i,j,k,l)$ depends on the kernel value of definite domain area

$$KL(i,j,k,l) = e^{\left[-\frac{(i-k)^2+(j-l)^2}{2\mu_{KL}^2}\right]} \quad (10)$$

and the value kernel

$$VL(i,j,k,l) = e^{\left[-\frac{\|PV(i,j)-PV(k,l)\|^2}{2\mu_{VL}^2}\right]} \quad (11)$$

respectively. Eventually, the total weight parameter is provided with the calculation of multiplying the last two equations and obtained as,

$$W_g(i,j,k,l) = e^{\left\{-\left[\frac{(i-k)^2+(j-l)^2}{2\mu_{KL}^2}+\frac{\|PV(i,j)-PV(k,l)\|^2}{2\mu_{VL}^2}\right]\right\}} \quad (12)$$

It is known that the assessment for the ways of feature extraction is much easier when the basic theories of combining the SS with the Bilaterial filter is adopted. On the other hand, the statement of SS and Bilaterial filter is quite suitable to apply to preserve the edge area and denoise for the clean the blur occurring in an image of WT blade.

## 5. The discussion of experiments and results

When using many skills to carry out the pre-processing of the WT blades, such as the combination of SS with Bilaterial Filter. This session will set up the experimental environment for identifying and predicting the possible damage or deterioration of WT blades with high accuracy. Some of the results of the experimental classification will also be discussed in this section.

Currently, the experiment of the proposed algorithm in this study is being carried out. The whole framework of pre-trained Tensorflow_keras Resnet-50 is shown in Fig. 6, which is used in the process of experiment for image pre-processing [19]. The different types of WT blade are described in Sec. III, where the dataset of WT blade is divided into four types. Another method of damage assessment is the

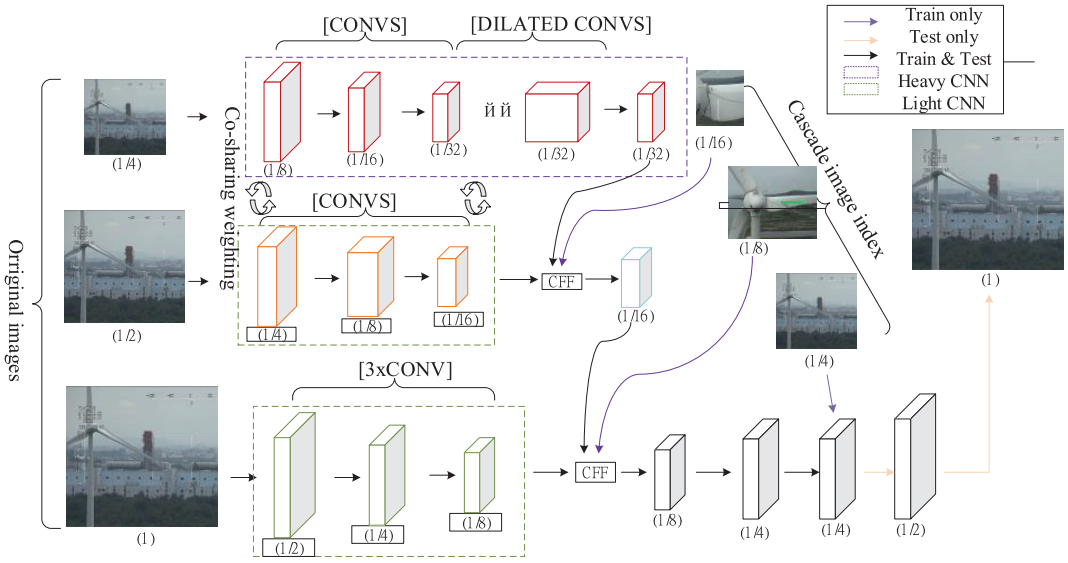


*Fig. 6. The whole framework of pre-trained Tensorflow_keras Resnet-50.*

regular or cracked process, which is implemented by the methods proposed in the current article. In the following, Table II lists the deployment of hyperparameters applied to the adopted NN framework to repeat the experiments. It is easy to observe from Table II that the items of hyperparameters are “Pixel Size #", “Class #", “Epochs #", “Freeze Layer #", “Batch Size #". The ratio of the selected data set to the establishment of the trained model with ML is 7 to 3. In the process of deployment to the architecture of NN there are the distribution graphs of the input layer, hidden layer and output layer of the RESNET-50 model. After the trained model is built, it can be learned through deep learning adaptive training and in the process of validation and testing stages.

Although the video of collecting WT blades in time could not be presented in the context of the article, the training step is still able to be expressed with text. So far, after learning the model is obtained to generate the ML framework for the work of testing with the filename of model-resnet50-final.h5. The building block model performs data processing and divides the data into normal and damaged images in the first step. First, the individual input images are analyzed by 5280 times 2970, and then the regular images are reshaped into 224x224 images. Specifically, at the image acquisition stage, a total of 1270 images including normal and damaged images are provided with image pre-processing. During the training stage to build the deep learning model, the accuracy rate and loss rate are shown in Fig. 7 (A) and (B), respectively.

The image is then split and divided into the corresponding type A and type B worn images. In addition, the normal images are also retained after classification. Finally, there are some images with severe background noise that cannot be removed, and they are classified as unknown images, called type-D images. The results of the final experiments can be obtained to verify the validity of the pre-processed images.

YOLO's convolutional network architecture is a model of GoogleNet. YOLO's network has 24 convolutional layers and 2 layers of fully connected layers [27]. The difference from GoogleNet is that in some $3 \times 3$ the author uses a $1 \times 1$ convolutional layer before the convolutional layer to reduce the number of filters. For validation purposes, the YOLOv4 neural network is used as the model to train the corrective action of the image pre-processing. In the process of real-time WT blade image acquisition, it can be seen that when the UAV is close to the WT blade, the camera always targets and marks the damaged part in the WT blade. No matter its size, spot or regular, the captured WT blades are immediately retrieved including the abnormal parts. The retrieval and storage actions then follow the previous image acquisition steps.

*Table 2. Hyperparameters applied to the RESNET-50 model.*

| Hyperparameter items | Learn rate | Pixel size | Class # | Epochs # | Freeze Layers # | Batch size # | Dropout rate |
|---|---|---|---|---|---|---|---|
| Deployed number | 0.001 | (224, 224) | 2 | 80 | 2 | 8 | 7:3 |

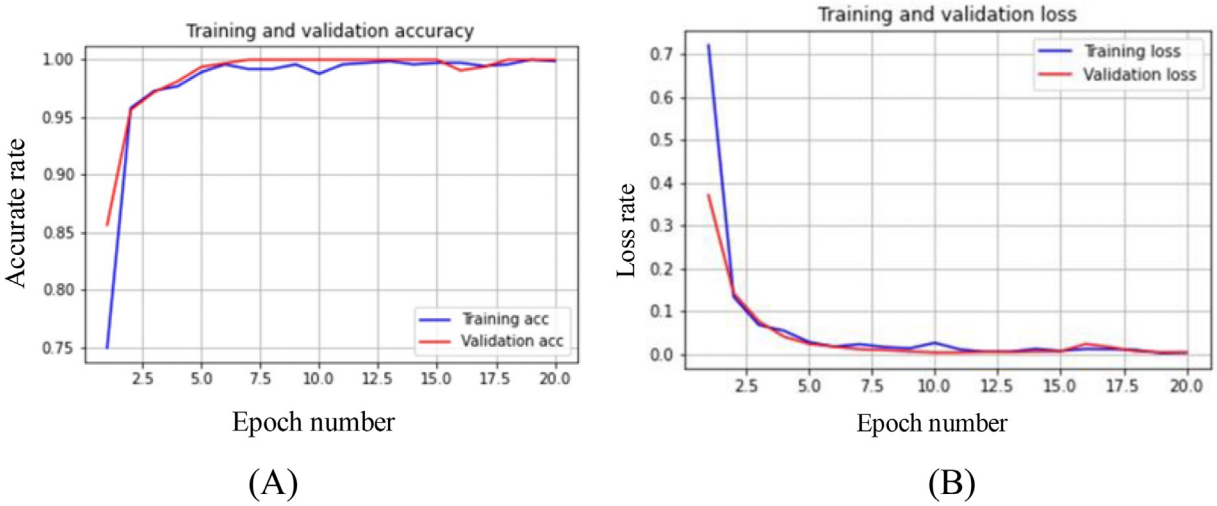


*Fig. 7. The loss rate of training model with ResNet50 NN.*

Furthermore, the hypermeters to be used to implement the YOLOv4 framework, which will be completed later, are shown in Table III. In the given table, where includes the hardware environment, software version and training network parameters for this experiment, and which can look in depth into the inspection of the repetition for the experiments hyperparameters in. Accordingly, there the Model-1 and Model-2 are implemented in the proposed algorithms to validate the training framework comes from the Resnet-50, and they are corresponding to the YOLOv4-Tiny and YOLOv4 models. On the other hand, the former and later are designed for the edge computing device of YOLOv4-Tiny and traditional YOLOv4 models, respectively.

As this article is a practical project, the feasibility of future commercial transfer should be considered. Therefore, the deep learning model with a recognition rate of more than 90 % is finally transplanted to Nvidia Jetson Nano as a basis for edge computing, which is available for commercial migration for large-scale UAV applications in the future. The application scenario is shown in Fig. 8 [20,25].

In this research, a Generative Adversarial Network (GAN) was imported into the data preprocessing part to generate a set of virtual defect photos, and combined with real photos, a YOLO deep learning model was established to achieve 95 % blade defect recognition.

Finally, download the algorithm module to the NVIDIA Jetson Xavier NX development version, as shown in Fig. 9. In fact, the installed edge devices of Jetson Nano could be replaced with other available options, such as the edge MCU with STM series, Arduino or even the Raspberry@ modular. That's why the type of available edge devices definitely depends on the computing speed and working

*Fig. 8. A photo for real-time capturing to the image of the WT blade.*

*Table 3. Hyperparameters applied to the YOLOv4 models.*

| Hyperparameter items | Hardware environment: Windows 10/RAM: 128GB/GPU: NVIDIA 1080 | | | | | | |
|---|---|---|---|---|---|---|---|
| | Optimizer: Adam | | | | | | |
| | Deployed numbers | | | | | | |
| | Learn rate | Pixel size | Class # | Epochs # | Freeze Layers # | Batch size # | Dropout rate |
| Model-1 (YOLOv4-Tiny) | 0.0025 | (448,448) | 2 | 6000 | 1 | 64 | 7:3 |
| Model-2 (YOLOv4) | 0.0025 | (448,448) | 2 | 10000 | 1 | 64 | 8:2 |

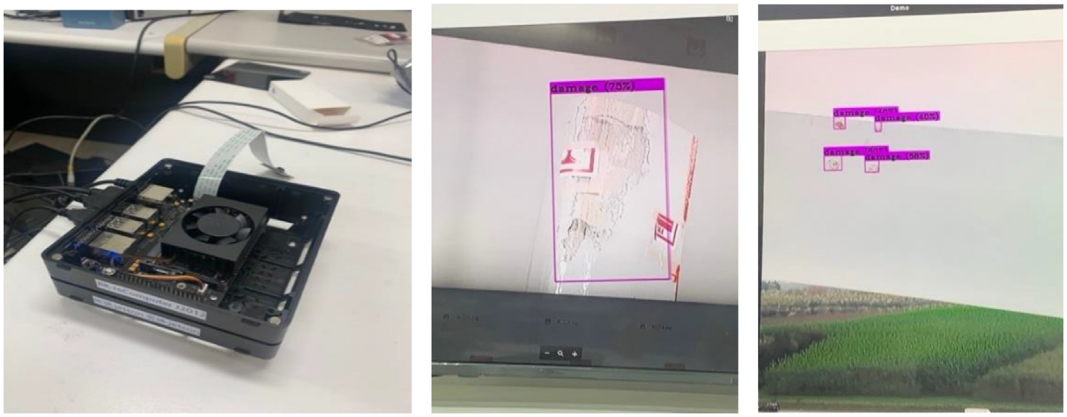

*Fig. 9. The NVIDIA Jetson Nano Xavier NX development version.*

efficiency. The flow continued by actually applying the training model to the NVIDIA Jetson Xavier NX development board combined with the Raspberry Pi Camera v2 lens, we put the image of the damaged fan blade on the screen, install the trained YOLOv4 model and add the lens through the GPU-accelerated operation on the development board. Real-time image recognition is performed on the data returned by the terminal.

In the recognized streaming screen, YOLOv4-Tiny can reach 32FPS and the recognition rate can reach more than 70 %. However, in YOLOv4, it can present 26FPS images, and the actual recognition rate can reach 80 %. Contrary to the above issue, YOLOv4-Tiny can actually accurately identify the damaged area of the blade. Obviously, although the original image resources are limited, the GAN in this study can still generate high resolution simulated images.

Specifically, 329 photos were used to build the framework after model training in the two training times. From the comparison of them with each other from the point of view of error, the lightweight model YOLOv4-Tiny is much faster than YOLOv4-Tiny in terms of training time. The average target detection evaluation index (mAP) of YOLOv4-Tiny has a larger fluctuation, reaching 90 % after 5000 times, but remaining 88 % in the final training result (85 % without GAN image). The error of YOLOv4-Tiny starts to oscillate after 400 iterations. After 3000 training times, the average target detection

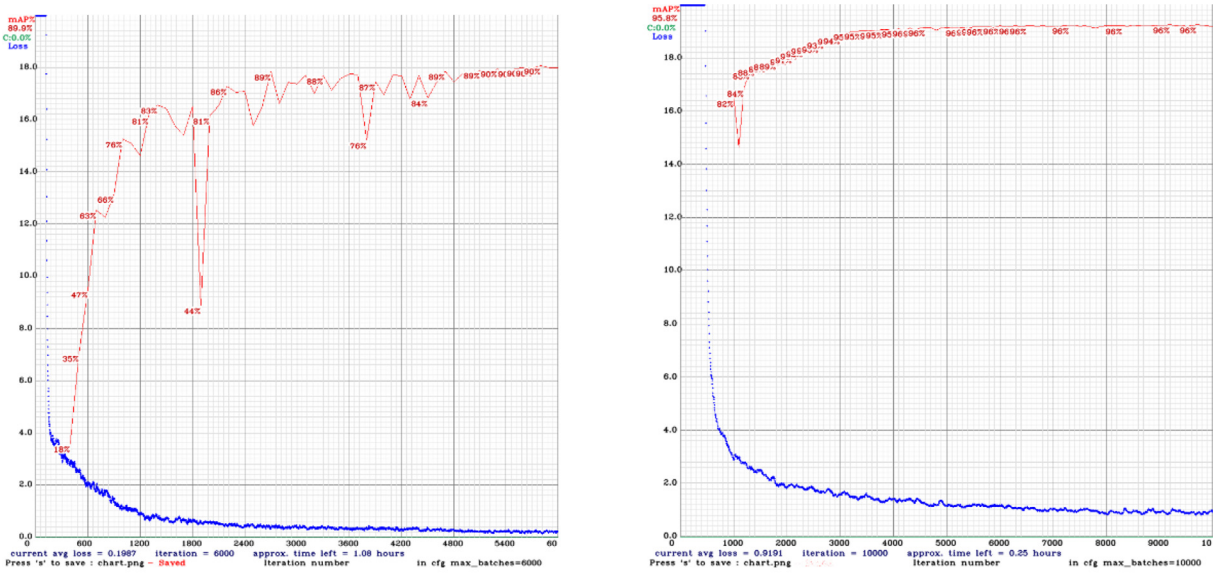


(A) (B)

*Fig. 10. (A). For YOLOV4-Tiny model, and (B). For YOLOv4 model.*

evaluation index stabilizes at 94 % (92 % without GAN images) and reaches a maximum of 96 % after 4000 times. The final training result remains at 95 %, and the reason for this can be discussed later. Two training results show that YOLOv4-Tiny has a higher recognition rate, as shown in Fig. 10 (A). Two training results show that YOLOv4 has a higher recognition rate, as shown in Fig. 10 (B).

## 6. Conclusion

An image pre-processing operation platform for complete machine learning image data has been proposed in the article. A machine learning algorithm with high accuracy classification efficiency has been developed for WT blade defect classification. In addition, a high-efficiency and high-accuracy deep learning algorithm for WT blade defect identification is developed and validated based on the YOLO framework (combined with GAN virtual graphics). The simulation report of the fire caused by the WT disaster has been completed. Therefore, the key hazard factors of the WT blades can be definitively defined after the completion of a WT disaster risk assessment report. In addition, the deep learning visual recognition model has been established and installed on the Nvidia Jetson Nano edge computing module, which can easily realize real-time image recognition and even continue to be a commercial transfer prototype.

## Conflict of interest

The authors declare no conflict of interest.

## References


[1] Drone market outlook in 2021. Accessed: Nov. 1, 2021. [Online], https://www.businessinsider.com/drone-industry-analysis market-trends-growth-forecasts.

[2] Accessed: Nov. 1, 2021. [Online], https://www.bnext.com.tw/article/65236/offshorewind-2021.

[3] Zhang J, Cosma G, Watkins J. Image enhanced Mask R-CNN: a deep learning pipeline with new evaluation measures for wind turbine blade defect detection and classification. J. Imaging 2021;7(No. 3). https://doi.org/10.3390/jimaging7030046.

[4] Yan X, Wu G, Zuo Y. YOLOV4-Based wind turbine blade crack defect detection. Proceedings of IncoME-VI and TEPEN 2021. Mechanisms and Machine Science 2021;117:293−305. https://doi.org/10.1007/978-3-030-99075-6_25.

[5] Kartik C, Nevena S, Elizabeth JC, Nikolaos D, Keith W. Damage detection in operational wind turbine blades using a new approach based on machine learning. Renewable Energy; May 2021. p. 1249−64. https://doi.org/10.1016/j.renene.2020.12.119. 168.

[6] Diaz PM, Tittus P. Fast detection of wind turbine blade damage using cascade Mask R-DSCNN-aided drone inspection analysis," signal, Image and video processing. Jan. 2023. p. 2333−41. https://doi.org/10.1007/s11760-022-02450-6. 17.

[7] Wang L, Zhang Z, Long H, Xu J, Liu R. Wind turbine gearbox failure identification with deep neural networks. IEEE Trans Ind Inf 2017;13(No. 3):1360−8.

[8] Qiu Z, Wang S, Zeng Z, Yu D. Automatic visual defects inspection of wind turbine blades via YOLO-based small object detection approach. J Electron Imag 2019;28(No. 4):043023.

[9] Wilson AN, Kumar A, Jha A, Cenkeramaddi LR. Embedded sensors, communication technologies, computing platforms and machine learning for UAVs: a review. IEEE Sensor J 2022;22(No. 3). Feb. 1.

[10] Mustafa Z. Classification of UAV point clouds by random forest machine learning algorithm. Turkish Journal of Engineering April 2021;5(2):51−61.

[11] Wang CX, Tian JM, Cao JW, Wang XH. Deep learning-based UAV detection in pulse-Doppler radar. IEEE Trans Geosci Rem Sens 2022;60:5105612−24.

[12] Li WB, Hu B, Song C, Zhao F, Ma HL, Wang YJ. An image stitching method for blades of wind turbine based on background removal preprocessing," *Proceeding of 5th international Conference on communication, Image and signal processing* (CCISP). June 2021. p. 174−9.

[13] Xu DH, Wen CB, Liu JH. Wind turbine blade surface inspection based on deep learning and UAV-taken images. J Renew Sustain Energy 2022. https://doi.org/10.1063/1.5113532 [Online]March. 20.

[14] Zhang NN, Lu CZ. Wind turbine blade defect image acquisition system. J. Phys.: Conf. Ser. 2020;1646:012086. 1-6.

[15] Shaw J, Wu BJ. Prediction of remaining useful life of wind turbine shaft bearings using machine learning. J Mar Sci Technol 2021;29. https://doi.org/10.51400/2709-6998.2465. 5, Article 4.

[16] Mao Y, Wang S, Yu D, Zhao J. Automatic image detection of multi-type surface defects on wind turbine blades based on cascade deep learning network. Intell Data Anal 2021;25(No. 2):463−82.

[17] Zhang R, Wen C. SOD-YOLO: a small target defect detection algorithm for wind turbine blades based on improved YOLOv5. Advanced Theory and Simulations 2022:2100631.

[18] Redmon J, Divvala S, Girshick R, Farhadi A. You only look once: unified, real-time object detection. In: Proceedings of the IEEE conference on computer vision and pattern recognition; 2016. p. 779−88.

[19] Rahmat N, Nur AF, Muhammad D, Muhammad H. Correlation of safety perceptions and safety behavior in university teaching laboratory. Malaysian Journal of Public Health Medicine 2020;20(No. 1):1−5.

[20] Huang S. Current status and prospects of marine energy development in taiwan. Marine Research, Trial Issue 2020:25−34.

[21] Wang L, Long H, Zhang Z, Xu J, Liu R. Wind turbine gearbox failure monitoring based on SCADA data analysis. Proc. IEEE Power Energy Soc. Gen. Meeting 2016:1−5.

[22] https://blog.csdn.net/MoFMan/article/details/77482794.

[23] David HA. Order statistics. New York: John Wiley & Sons, Inc.; 1981.

[24] Ashiba HI, Mansour HM, Ahmed HM. Enhancement of infrared images based on efficient histogram processing. Wireless Pers Commun 2018;99:619−36.

[25] Shafiee M, Zhou Z, Mei L, Dinmohammadi F, Karama J, Flynn D. Unmanned aerial drones for inspection of offshore wind turbines: a mission-critical failure analysis. Robotics 2021;10(No. 1):26.

[26] Islam M, Laskar RH. Geometric distortion correction based robust watermarking scheme in LWT-SVD domain with digital watermark extraction using SVM. Multimed. Tools 2018;77:14407−34.

[27] Redmon J, Divvala S, Girshick R, Farhadi A. You only look once: unified, real-time object detection. IEEE Conference on Computer Vision and Pattern Recognition 2016:779−88.

[28] Accessed: July. 1, 2022. [Online], https://viso.ai/deep-learning/resnet-residual-neural-network/.